ARCHIVES OF ELECTRICAL ENGINEERING VOL. 71(1), pp. 109–124 (2022)

DOI 10.24425/aee.2022.140200

An approach to suppress low-frequency oscillation in the hybrid multi-Infeed HVDC of mixed H_2/H_∞ robust-based control theory

CONGSHAN LI ✉, YAN LIU, YIKAI LI, PING HE, YAN FANG, TINGYU SHENG

School of Electrical and Information Engineering, Zhengzhou University of Light Industry China

e-mail: 543627767@qq.com

(Received: 25.05.2021, revised: 30.09.2021)

Abstract: A hybrid multi-infeed HVDC (HMIDC) system is composed of line-commutated converter-based high-voltage direct current (LCC-HVDC) and voltage-source converter-based high-voltage direct current (VSC-HVDC), whose receiving ends have electrical coupling. To solve the problem of low-frequency oscillation (LFO) caused by insufficient damping in the HMIDC system, according to the multi-objective mixed H_2/H_∞ output feedback control theory with regional pole assignment, an additional robust damping controller is designed in this paper, which not only has good robustness, but also has strong adaptability to the change of system operation mode. In the paper, the related oscillation modes and transfer function of the controlled plant are obtained, which are identified by the total least squares estimation of signal parameters via rotary invariance technology (TLS-ESPRIT). In addition, the control-sensitive point (CSP) for suppressing LFO based on the small disturbance test method is determined, which is suitable for determining the installation position of the controller. The results show that the control sensitivity factor of VSC-HVDC is greater than that of LCC-HVDC so that adding an additional damping controller to VSC-HVDC is better than LCC-HVDC in suppressing the LFO of HMIDC. Finally, a hybrid double infeed DC transmission system with three receiving terminals is built on PSCAD/EMTDC where the time-domain simulations are performed to verify the correctness of the CSP selection and the effectiveness of the controller.

Key words: additional damping controller, CSP, HMIDC, LFO, mixed H_2/H_∞ control, TLS-ESPRIT

1. Introduction

In the field of power transmission, the line-commutated converter-based high-voltage direct current (LCC-HVDC) occupies half of the territory due to its advantages of trans-regionality, long-distance coverage and bulk power [1]. As the latest generation of transmission technology, voltage-source converter-based high-voltage direct current (VSC-HVDC) has gradually penetrated into the field of transmission and has great application potential in clean energy accommodation. Therefore, future power grids will inevitably have multiple LCC-HVDC and VSC-HVDC feeds into the same or nearby electrical distance systems, which will ultimately form a hybrid multi-infeed HVDC (HMIDC). For example, the Skagerrak HVDC Interconnection Pole 4 project between Norway and Denmark adopted VSC-HVDC to form a hybrid four-pole HVDC system based on the original three-pole LCC-HVDC, which presents the HMIDC system shape on the receiving end [2]. The HMIDC system has the advantages of both LCC-HVDC and VSC-HVDC and is a new type of HVDC topology. It is well known that interconnected transmission systems are prone to produce low-frequency oscillations (LFOs) when subjected to small disturbances. LFO is a typical problem for power systems that causes the transmission capacity of HVDC systems to decrease, and power systems can lose stability if this condition is improperly processed.

Various control techniques have been used to increase the damping ratio to suppress the LFO for power systems, such as power system stabilizers (PSSs) [3–6], flexible AC transmission systems (FACTSs) [7–9], and the additional damping control of HVDC [10, 11]. The high controllability and fast response characteristics of HVDC can be used to damp LFO by adding supplementary control on the basis of original control, which was noted in [12–22]. In [12], an additional damping controller for LCC-HVDC provided by the multilevel linear optimal method has the advantages of good adaptability. However, it has a higher controller order, which is not suitable for engineering in practice. In [13], a multichannel additional robust controller for multiple LCC-HVDC was designed using the linear matrix inequality (LMI) method, which possessed strong robustness. In [14], a supplementary LCC-HVDC controller based on model predictive control (MPC) provided faster recovery times after faults compared with a linear quadratic Gaussian (LQG)-based controller. Because VSC-HVDC stations can operate as virtual synchronous machine (VSM) to suppress LFO [15], we investigated how a VSM affects LFO in power systems by analyzing the equivalent damping torque and showed that VSM can provide considerable positive damping torque. Reference [16] presented a novel combined design of VSC-HVDC and PSS controllers to enhance the damping of the power system. Wide area measurement systems (WAMSs) are increasingly applied in large-scale power systems, so the wide area damping control of HVDC to suppress LFOs has become the subject of considerable attention among many researchers [17–19]. In [17], a wide-area multi-HVDC damping controller based on power system state space model identification of auto regressive exogenous was designed to improve damping efficiently. In [18], a shaped loop transmission function was verified to effectively improve the noise response which had strong adaptability. In [19], a control strategy for multiple embedded dc links was proposed to make the system in nontarget mode have better robustness.

In addition, a few references have focused on controlling sensitive point (CSP) digging for suppressing LFO in multiple HVDC systems [20–22]. Although the schemes for suppressing LFO are well presented in these references, these schemes are only applicable to power systems consisting purely of LCC-HVDC or VSC-HVDC.

At present, few scholars have carried out research on a HMIDC system for suppressing LFO. Compared with the aforementioned references, this paper designs an additional damping controller that is relatively easy to implement in practical engineering and proposes a method for determining a CSP suitable for the installation position of the additional controller. The main research contents of this paper are as follows:

1. Firstly, the oscillation modes and transfer function of the controlled plant are identified by the total least squares estimation of signal parameters via rotary invariance technology (TLS-ESPRIT).
2. Secondly, to address the control-sensitive point of LFO for HMIDC, this paper uses the small disturbance test method to select the control-sensitive point, which has the best suppression effect on the LFO.
3. Thirdly, according to the multi-objective mixed H_2/H_∞ output feedback control theory with regional pole assignment, an additional robust damping controller is designed. In addition, the balanced truncation method is adopted to reduce the order of the controller to avoid problems that are not easily applied in practical engineering due to the high order of the controller.
4. Finally, the time-domain simulations are used to verify the correctness of the CSP selection and the effectiveness of the controller in a hybrid dual-infeed HVDC system.

2. Analysis of LFO characteristics for the HMIDC system based on TLS-ESPRIT

Modal analysis is one of the classic methods used for studying LFO in power system, which is also known as eigenvalue analysis. To restrain the LFO, it is first necessary to accurately identify the modes of LFO. In this paper, the TLS-ESPRIT is used to accurately identify the oscillation mode.

TLS-ESPRIT is an improvement of ESPRIT and is a high-resolution subspace-based signal analysis method [23]. It is especially suitable for the analysis of oscillation characteristics and model identification under a large system with small disturbances.

The design of an additional damping controller requires an exact mathematical model. To obtain the parameters of the controller, a linearized model of the controlled plant must be acquired. The hybrid dual-infeed HVDC system mode shown in Fig. 1 is initiated to identify the oscillation characteristics. The subsystem of the LCC-HVDC is modified from the CIGRE standard test model, and its control blocks are consistent with the CIGRE model. The CIGRE standard test model is detailed in reference [24]. In addition, primary parameters of the LCC-HVDC subsystem and VSC-HVDC subsystem are showed in the Table 1 and Table 2 in detail. The subsystem of VSC-HVDC employs vector current control (VCC) with direct current control based on a synchronous rotating reference frame d–q. The constant AC voltage and constant active power control are adopted in the rectifier, and the constant DC voltage and constant AC voltage control are employed in the inverter.

After the system shown in Fig. 1 accesses the steady state, a small disturbance excitation that does not damage the linearization of the system is applied. In this research, a power disturbance of 0.02 pu times to the LCC-HVDC is selected for the input signals, and rotor angular velocity

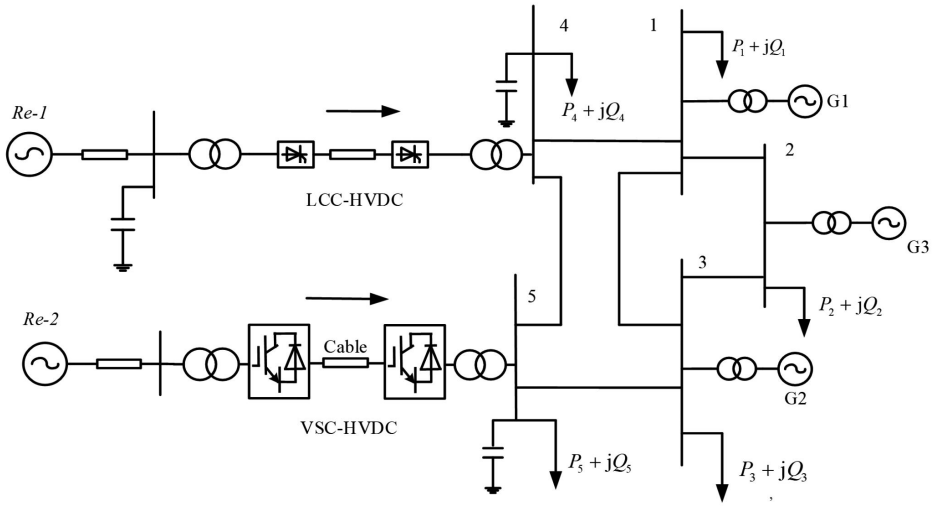

Fig. 1. Hybrid dual-infeed HVDC system

where Re_1 and Re_2 are the equivalent AC systems of the LCC-HVDC and VSC-HVDC, respectively; G_1, G_2 and G_3 are the generators of the receiving AC system; and $P_{Li} + Q_{Li}$ is the load. L is the electrical distance, which is represented by a π-type equivalent circuit.

Table 1. Primary parameters of LCC-HVDC subsystem

The LCC parameters	Rectifier side	Inverter side
Equivalent AC system	328.87 kV	215.05 kV
Converter transformer capacity	603 MW	591.8 MW
Conversion ratio of transformer	345/213.5 kV	340/209.2 kV
Smoothing reactor	0.5968 H	0.5968 H

Table 2. Primary parameters of VSC-HVDC subsystem

The VSC parameters	Rectifier side	Inverter side
Equivalent AC system	215.05 kv	230 kv
Converter transformer capacity	900 MW	800 MW
Conversion ratio of transformer	230/100 kV	230/150 kV
DC capacitance	1000 uF	1000 uF

deviation of each generator is taken as an output signal. The time-domain simulation data of the output signals for the before and after disturbance are sampled, we can identify the sampling data through the TLS-ESPRIT, and the identified oscillation modes are given in Table 3.

Table 3. The modes of oscillation

	Oscillations	**Eigenvalue**	**Frequency (Hz)**	**Damping Ratio (ξ %)**
ω13	mode1	$-0.1163 + 10.1011i$	1.6076	1.15
	mode2	$-0.3424 + 7.3483i$	1.1695	4.65
	mode3	$-0.67836 + 3.03852i$	0.4836	21.79
ω12	mode1	$-0.2504 + 10.2408i$	1.6299	2.44
	mode2	$-0.3146 + 7.3392i$	1.1681	4.28
	mode3	$-0.5915 + 2.9783i$	0.4740	19.48
ω23	mode1	$-0.0608 + 10.6694i$	1.6981	0.57
	mode2	$-0.1063 + 7.3505i$	1.1699	1.45
	mode3	$-0.6196 + 2.9486i$	0.4963	20.56

It can be seen from Table 3 that the system mainly participates in the local oscillation modes of approximately 1.60 Hz and 1.1 Hz, and the damping ratios are close to zero. They all belong to the poorly damped oscillation modes to be suppressed, which are called the main oscillation modes. The system also participates in an inter-area mode of approximately 0.5 Hz, where the damping ratio is slightly higher than the local mode. A Butterworth bandpass filter with a frequency range of 0.8–1.7 Hz is added, and ω13 is taken as the identification target. Using the TLS-ESPRIT for identification again, the 6th-order transfer function G(s) of the controlled plant is shown in Eq. (1).

$$G(s) = \\ = \frac{-0.0024s^6+0.0710s^5+0.1254s^4+0.0580s^3}{s^6+2.6353s^5+66.6521s^4+125.2475s^3} \leftarrow \frac{+1.7289s^2+0.1276s}{+624.2779s^2+649.4768s+165.3277}. \tag{1}$$

3. Determination of the CSP for HMID

The multiple HVDC transmission system creates different damping effects by adding additional controllers at different HVDCs, so there is a problem of controlling sensitive point, consistent with the findings of [20, 21]. The CSP refers to the HVDC system that contributes the most to the damping degree of an oscillation mode in a power system with multiple HVDCs. Whether the CSP determined according to the control target is appropriate decides whether the DC modulation would achieve the intended effect. Reference [22] notes that the effect of an additional damping controller on suppressing LFO is related to the amplitude of the main oscillation mode when the input signal is given. This paper chooses the control sensitivity factor to select the CSP. The control sensitivity factor is defined as follows:

$$\rho = \frac{R}{\Delta P}, \tag{2}$$

where R is the amplitude of the frequency corresponding to the oscillation mode M; this paper applied ΔP as power interference and attached it to each DC power command value. It can be considered that the effect of controlling an HVDC line with a large sensitivity factor is better than the effect of other DC lines at suppressing this oscillating mode M. Taking $\omega 13$ as an example, the specific steps are as follows:

1. The main oscillation mode M of the system are identified through TLS-ESPRIT. Then, a power disturbance of ΔP is applied to each HVDC, and the rotor angular velocity change $\Delta\omega$ between strong correlation generators is measured.
2. TLS-ESPRIT is used to identify $\Delta\omega$ and find the amplitude R corresponding to the oscillation mode M. Based on Eq. (2), the control sensitivity factor is calculated. The HVDC line with a larger control sensitivity factor is the installation position of the additional damping controller.
3. If the system contains multiple main vibration modes, repeat the above steps to determine the CSPs for each vibration mode.

This paper applied a 2% power disturbance to the power command value of LCC-HVDC and VSC-HVDC and took out the time-domain simulation data of $\Delta\omega$ before and after disturbance. As per $\Delta\omega$, the frequencies and amplitudes of oscillation under different disturbances are identified in Table 4.

Table 4. Identification results under different disturbances

Disturbed case	Main oscillation	Oscillation amplitude
LCC-HVDC	1.6049	1.0489×10^{-6}
	1.1698	2.4949×10^{-4}
	0.7718	1.9296×10^{-6}
VSC-HVDC	1.5973	3.3354×10^{-6}
	1.1615	2.6492×10^{-4}
	0.8198	4.3872×10^{-6}

As shown in Table 4, regardless of the main oscillation frequencies, the control sensitivity factor of VSC-HVDC is greater than that of LCC-HVDC. It can be concluded that adding an additional damping controller to VSC-HVDC is better than LCC-HVDC in suppressing the LFO of HMIDC.

4. The mixed H_2/H_∞ controller design theory based on pole assignment in the conic sector region

4.1. Theory of mixed H_2/H_∞ control

Because designing a controller by using an easily measured output as a feedback signal does not require devising a complex state observer, it is easy to design a corresponding controller. Therefore, this paper uses an output feedback controller to configure the poles in the appropriate region. Therefore, the synthesis structure diagram of the mixed multi-objective robust controller is shown in Fig. 2.

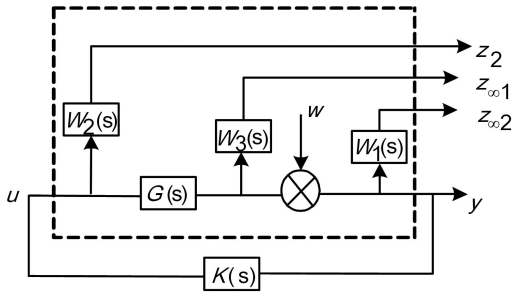

Fig. 2. Synthesis structure diagram of a multi-objective robust controller

where $G(s)$ is the transfer function of the controlled plant and $K(s)$ is the controller to be designed. $\boldsymbol{x}$, $\boldsymbol{u}$ and $\boldsymbol{y}$ are the vectors of state variables, control variables and output variables, respectively. w is the disturbance input, which represents the uncertainty factors of the system. $W_i(s)$ $(i = 1, 2, 3)$ is the weight function, the output channel $z_{\infty i}$ $(i = 1, 2)$ is associated with the performance H_∞, and the channel z_2 is associated with the performance H_2. Consider the power system depicted in Fig. 2 whose state space model is given by:

$$\begin{aligned} \dot{\boldsymbol{x}}(t) &= \boldsymbol{A}\boldsymbol{x}(t) + \boldsymbol{B}_1\boldsymbol{w}(t) + \boldsymbol{B}_2\boldsymbol{u}(t), \\ \boldsymbol{z}_\infty(t) &= \boldsymbol{C}_1\boldsymbol{x}(t) + \boldsymbol{D}_{11}\boldsymbol{w}(t) + \boldsymbol{D}_{12}\boldsymbol{u}(t), \\ \boldsymbol{z}_2(t) &= \boldsymbol{C}_2\boldsymbol{x}(t) + \boldsymbol{D}_{21}\boldsymbol{w}(t) + \boldsymbol{D}_{22}\boldsymbol{u}(t), \\ \boldsymbol{y}(t) &= \boldsymbol{C}_3\boldsymbol{x}(t) + \boldsymbol{D}_{31}\boldsymbol{w}(t) + \boldsymbol{D}_{32}\boldsymbol{u}(t), \end{aligned} \tag{3}$$

where $\boldsymbol{A}$, $\boldsymbol{B}$, $\boldsymbol{C}$ and $\boldsymbol{D}$ are all the parameter matrices of Eq. (3), $z_\infty = [z_{\infty 1} z_{\infty 2}]^T$.

It is assumed that the output-feedback controller $K(\mathrm{s})$ to be designed has the following form of state space:

$$\begin{cases} \boldsymbol{x}_k = \boldsymbol{A}_k\boldsymbol{x}_k(t) + \boldsymbol{B}_k\boldsymbol{y}_k(t) \\ \boldsymbol{y}(t) = \boldsymbol{C}_k\boldsymbol{x}_k(t) \end{cases}, \tag{4}$$

where $\boldsymbol{x}_k$ is the state variable vector, and $\boldsymbol{A}_k$, $\boldsymbol{B}_k$ and $\boldsymbol{C}_k$ are the state matrix, the matrix of control inputs, and the output matrix of the $K(s)$, respectively.

Substituting Eq. (4) into Eq. (3) to obtain the state-space model of the closed-loop system after adding the controller can be written as:

$$\begin{cases} \dot{\boldsymbol{x}}_h(t) = \boldsymbol{A}_h\boldsymbol{x}(t) + \boldsymbol{B}_h\boldsymbol{w}(t) \\ \boldsymbol{z}_\infty(t) = \boldsymbol{C}_{h1}\boldsymbol{x}(t) + \boldsymbol{D}_{h1}\boldsymbol{w}(t) \\ \boldsymbol{z}_2(t) = \boldsymbol{C}_2\boldsymbol{x}(t) + \boldsymbol{D}_{\mathrm{h}2}\boldsymbol{w}(t) \end{cases}. \tag{5}$$

For the controller $K(s)$ designed in this paper, the H_2/H_∞ performance is considered synthetically; it defines T_∞ and T_2 as the closed-loop transfer functions from w to z_∞ and z_2, respectively. The main task of the output-feedback controller $K(s)$ is as follows:

1. Pole assignment in a conic sector region

The method of pole assignment in a specified region can not only adapt to the uncertain performance of the system model and the change of operating conditions but also effectively

avoid the problem that the single dominant pole assignment may not be accurate due to the error of the system identification model. The frequently used pole assignment regions are symmetrical about the real axis in the complex plane and are usually described by a linear matrix inequality region named an LMI region. For a given LMI region $\boldsymbol{D}$, there are matrices $\boldsymbol{L} \in \boldsymbol{R}^{m\times m}$ and $\boldsymbol{M} \in \boldsymbol{R}^{m\times m}$ satisfying:

$$\boldsymbol{D} = \left\{ s \in \boldsymbol{C} \colon \boldsymbol{L} + s\boldsymbol{M} + \bar{s}\boldsymbol{M}^T < 0 \right\}, \tag{6}$$

where $\bar{s}$ and $\boldsymbol{M}^T$ represent the conjugate complex number and transpose matrix, respectively.

The conic sector region with a damping ratio ξ greater than $\cos\theta$, as shown in Fig. 3, is selected as the pole assignment region in this paper, and its eigenfunction is expressed as:

$$f_{\boldsymbol{D}}(z) = \begin{bmatrix} \sin\theta\,(s+\bar{s}) & \cos\theta\,(s-\bar{s}) \\ \cos\theta\,(s-\bar{s}) & \sin\theta\,(s+\bar{s}) \end{bmatrix}.$$

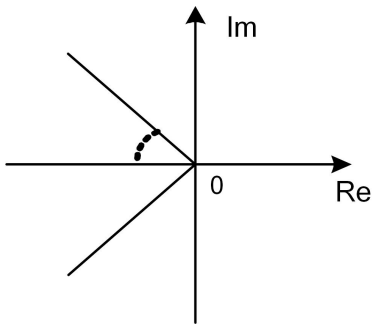

Fig. 3. LMI region $\boldsymbol{D}$ for pole placement

For the state matrix $\boldsymbol{A}_h$, the necessary and sufficient condition for all its eigenvalues to be in region $\boldsymbol{D}$ is that there is a symmetric positive definite matrix $\boldsymbol{X}$, which satisfies:

$$\boldsymbol{L} \otimes \boldsymbol{X} + \boldsymbol{M} \otimes (\boldsymbol{A}_h \boldsymbol{X}) + \boldsymbol{M}^T \otimes (\boldsymbol{A}_h \boldsymbol{X})^T < 0, \tag{7}$$

where $\otimes$ denotes the Kronecker product. The necessary and sufficient condition for the poles of the closed-loop system described in Eq. (5) to be all located in region $\boldsymbol{D}$ is that there is a positive definite matrix $\boldsymbol{X}_1$ that makes Eq. (8) work.

$$\begin{cases} \boldsymbol{A}_h \boldsymbol{X}_1 + \boldsymbol{X}_1 \boldsymbol{A}_h^T + 2\alpha \boldsymbol{X}_1 < 0 \\ \begin{bmatrix} \sin\theta \left(\boldsymbol{A}_h \boldsymbol{X}_1 + \boldsymbol{X}_1 \boldsymbol{A}_h^T \right) & \cos\theta \left(\boldsymbol{A}_h \boldsymbol{X}_1 - \boldsymbol{X}_1 \boldsymbol{A}_h^T \right) \\ \cos\theta \left(\boldsymbol{X}_1 \boldsymbol{A}_h^T - \boldsymbol{A}_h \boldsymbol{X}_1 \right) & \sin\theta \left(\boldsymbol{A}_h \boldsymbol{X}_1 + \boldsymbol{X}_1 \boldsymbol{A}_h^T \right) \end{bmatrix} < 0 \end{cases}. \tag{8}$$

1. H_∞ performance

If $\|\boldsymbol{T}_\infty\|_\infty < \gamma$, where γ is a given positive constant, then it can be ensured that Eq. (5) satisfies the robust performance corresponding to the upper bound γ for the uncertainties introduced by w. Based on the bounded real lemma, there exists a positive definite matrix $\boldsymbol{X}_2$, which makes Eq. (9) true.

2. H_2 performance

$$\begin{bmatrix} \boldsymbol{X}_2\boldsymbol{A}_h + \boldsymbol{A}_h^T\boldsymbol{X}_2 & \boldsymbol{X}_2\boldsymbol{B}_h & \boldsymbol{C}_{h1}^T \\ \boldsymbol{B}_h^T\boldsymbol{X}_2 & -\gamma\boldsymbol{I} & \boldsymbol{D}_{h1}^T \\ \boldsymbol{C}_{h1} & \boldsymbol{D}_{h1} & -\gamma\boldsymbol{I} \end{bmatrix} < 0. \tag{9}$$

To ensure that the control performance of the system measured by H_2 is at a good level, it is necessary to satisfy $\|\boldsymbol{T}_2\|_2 < \eta$, where η is a given positive constant. Similarly, there exist symmetric positive definite matrices $\boldsymbol{X}_3$ and $\boldsymbol{Q}$ satisfying:

$$\begin{cases} \begin{bmatrix} \boldsymbol{X}_3\boldsymbol{A}_h + \boldsymbol{A}_h^T\boldsymbol{X}_3 & \boldsymbol{X}_3\boldsymbol{B}_h \\ \boldsymbol{B}_h^T\boldsymbol{X}_3 & -\boldsymbol{I} \end{bmatrix} < 0 \\ \begin{bmatrix} \boldsymbol{X}_3 & \boldsymbol{C}_{h2}^T \\ \boldsymbol{C}_{h2} & \boldsymbol{Q} \end{bmatrix} \\ \mathrm{Trace}(\boldsymbol{Q}) < \eta^2 \end{cases}. \tag{10}$$

3. Multi-objective mixed H_2/H_∞ control

This can combine Eqs. (6)–(10) and make $\boldsymbol{X}_1 = \boldsymbol{X}_2 = \boldsymbol{X}_3 = \boldsymbol{X}$, and without the limitation of γ and η, the required robust controller $K(s)$ can be obtained by solving Eq. (11).

$$k(s)^{\min}\{\alpha\|T_\infty\|_\infty\} + \beta\|T_2\|_2 , \tag{11}$$

where α and β are the weight coefficients reflecting the H_∞ performance and H_2 performance, respectively, and $\alpha + \beta = 1$. In this paper, $\alpha = \beta = 0.5$ is selected. By using the hinfmix function in the LMI toolbox of MATLAB to calculate the parameters of $K(s)$, the transfer function can be obtained. The controller obtained through the above method can not only improve the system's damping but also provide robustness and optimal performance and achieve the optimal comprehensive performance of the controller.

4.2. Design of additional robust controller

An appropriate weight function must be selected when designing an additional robust controller for the sake of making the H_∞ and H_2 performance of the controller meet the expected requirements. In general, the order of the weight function should not be too high. $W_1(s)$ has a low-pass characteristic, $W_2(s)$ can be set as a small constant, and $W_3(s)$ has a high-pass characteristic and does not overlap with the frequency band of $W_1(s)$. The weight function selected in this paper is shown in Eq. (12):

$$\begin{cases} W_1(s) = \dfrac{1}{s+100} \\ W_2(s) = 1 \\ W_3(s) = \dfrac{0.01s}{s+100} \end{cases}. \tag{12}$$

Given the weight function for $G(s)$, a pole assignment region with a damping ratio greater than 25% is selected; let $\alpha = \beta = 0.5$ of Eq. (11), and without the restrictions of γ and η. The

output feedback controller is the additional damping controller as shown in Eq. (13):

$$K(s) = \left(-107.28s^7 - 2.13\times10^4 s^6 - 1.04\times10^6 s^5 + 2.53\times10^6 s^4 + 5.09\times10^7 s^3 + \right.$$
$$+ 2.75\times10^8 s^2 + 2.68\times10^8 s + 6.62s\left.\right) / \left(s^8 + 212.85s^7 + 1.27\times10^4 s^6 + 1.50\times10^5 s^5 + \right. \quad (13)$$
$$\left. + 1.16\times10^6 s^4 + 4.09\times10^6 s^3 + 9.44\times10^6 s^2 + 7.08\times10^6 s + 1.66\times10^6\right).$$

It can be observed from Eq. (13) that the order of the output feedback controller is higher, which is not conducive to practical application. In this paper, the balanced truncation method based on Hankel singular value decomposition is performed to reduce the order of the controller, which the fourth-order output feedback controller gives as follows:

$$K_r(s) = \frac{-110.37s^3 + 532.95s^2 + 1.95\times10^3 s + 2.41\times10^4}{s^4 + 10.27s^3 + 80.86s^2 + 252.92s + 602.44}. \quad (14)$$

For LCC-HVDC, an additional damping controller is added at the rectifier constant current control. The structure is shown in Fig. 4.

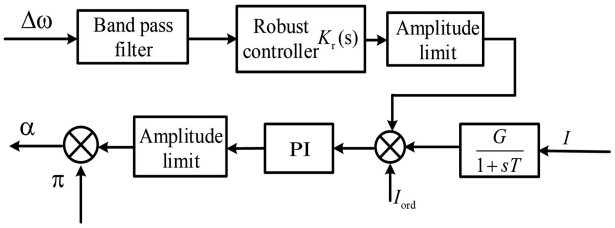

Fig. 4. The structure of constant current control with additional controller for LCC-HVDC

For VSC-HVDC, an additional damping controller is installed at the constant active power control on the rectifier. The structure is shown in Fig. 5.

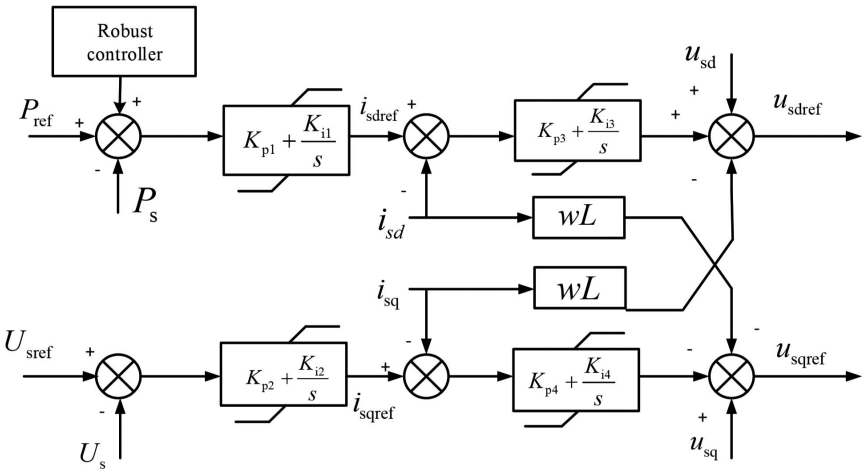

Fig. 5. The structure of *dq*-based control with robust controller for VSC-HVDC

5. Case study and discussion

5.1. Verification of the control sensitive point

At 2 s, a single-phase ground fault occurs at bus 4, and the fault clears after 0.1 s. Taking the rotor angular velocity deviation $\Delta\omega 13$ as control objectives, without an additional damping controller, LCC-HVDC and VSC-HVDC add additional damping controllers; In addition, the inverter side in LCC-HVDC subsystem where the short-circuit ratio is about 3.68 adopts constant DC current control and constant gama control. The simulation results are shown in Fig. 6.

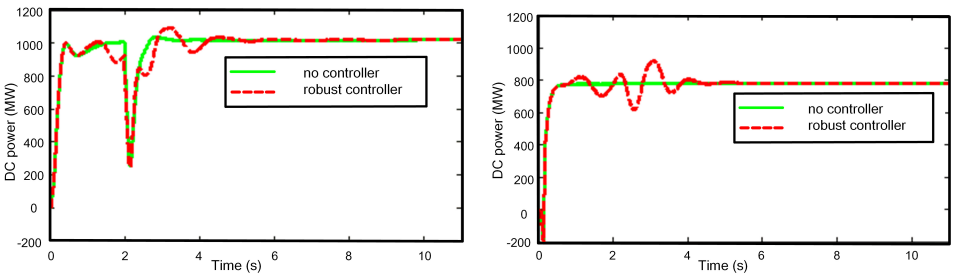

Fig. 6. The DC power curve of damping modulation with different HVDC: the DC power amount of LCC-HVDC (a); the DC power amount of VSC-HVDC (b)

Fig. 6 shows that when a short-circuit fault occurs on bus 4, the voltage of the LCC-HVDC is greatly affected by the fault, and the DC power transmitted is decreased. VSC-HVDC is insensitive to faults, which indirectly proves that the stability of the system can be improved after VSC-HVDC is fed to the HVDC system. Moreover, Fig. 6 also shows that the maximum power modulation amount of LCC-HVDC and VSC-HVDC is approximately 100 MW. At the same time, it can be observed from Fig. 7 that both the VSC-HVDC and LCC-HVDC additional damping control can reduce the amplitude of the first swing and increase the damping of the subsequent swing, which can suppress the system oscillation to a certain extent. In the case of the same power modulation amount, the additional damping control of VSC-HVDC is slightly more than the additional damping control of LCC-HVDC in increasing the damping of subsequent swing aspect, which verifies the correctness of the selection of the CSP.

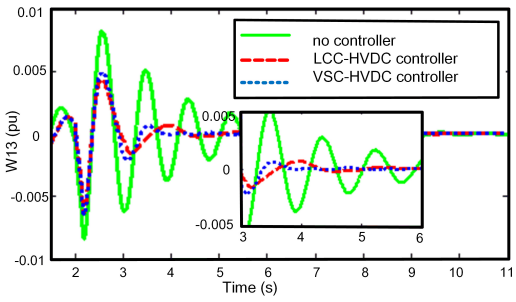

Fig. 7. $\Delta\omega 13$ under different HVDC with additional robust damping controller

5.2. Control effect and robustness verification of an additional damping controller

To verify the damping effect and robustness of the additional robust damping controller designed in this paper, it is compared with the additional damping controller compensated by the root locus method. The setting of the bandpass filter and limiting link is identical to the additional robust damping controller. The series lead correction network is selected to compensate for the original system, and the series correction network is converted to the negative feedback loop. Balance truncation is also employed to reduce the order of the controller. The damping ratio of the system is selected to improve to 0.25, and the natural oscillation frequency is adjusted to 2 rad/s. In other words, the dominant pole of the system will be corrected to $-0.5 + 1.936i$, and the final reduced root locus damping controller is as follows:

$$\begin{aligned} H(s) = \big(&- 412.8s^8 + 4333s^7 - 1.4 \times 10^4 s^6 + 3.1 \times 10^5 s^5 + 3.2 \times 10^5 s^4 + 2.9 \times 10^6 s^3 + \\ &+ 2.4 \times 10^6 s^2 - 1.7 \times 10^5 s - 2.7 \times 10^5 \big) / \big(s^8 - 42.6s^7 + 340.3s^6 + \\ &+ 321s^5 + 2346s^4 + 8153s^3 - 3553s^2 + 210.8s - 1.2 \times 10^{-15} \big). \end{aligned} \tag{15}$$

Case 1: At 2 s, bus 5 suddenly loses the load, the fault is automatically removed after 0.5 s, and the root locus controller and the robust controller are put into the active power control link of VSC-HVDC. Taking $\Delta\omega 12$, $\Delta\omega 13$ and $\Delta\omega 23$ as observation objects, the simulation results are shown in Fig. 8.

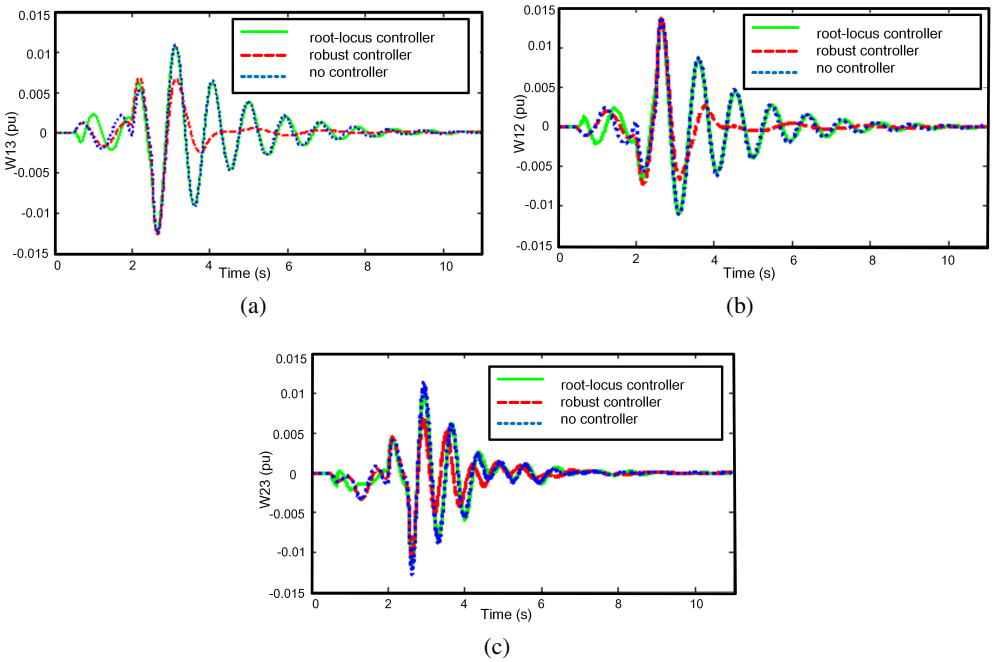

Fig. 8. Comparison of the control effect before and after the controller installation in case 1: comparison of the control effect based on $\omega 13$ (a); comparison of the control effect based on $\omega 12$ (b); comparison of the control effect based on $\omega 23$ (c)

The simulation results in Fig. 8 indicate that the generator speed changes after the system is subjected to a small disturbance, and the system will continue to oscillate if there are no control measures. After the root locus controller is installed, the amplitude of the first swing is reduced, and the oscillation is restrained to a certain extent, but the increase in the damping of the subsequent swing is not obvious. The robust controller can calm down the system oscillate faster, which not only reduces the amplitude of the first swing but also increases the damping of the subsequent swing significantly more than the root locus controller. Therefore, it can be concluded that the damping effect of the robust controller on LFO is better than that of the root locus controller.

Case 2: At 2 s, a transient three-phase metallic short-circuit fault occurs at bus 3, the ground resistance is 0.01 Ω, and the fault clears after 0.3 s. The rest of the settings are the same as in case 1. The simulation results are shown in Fig. 9.

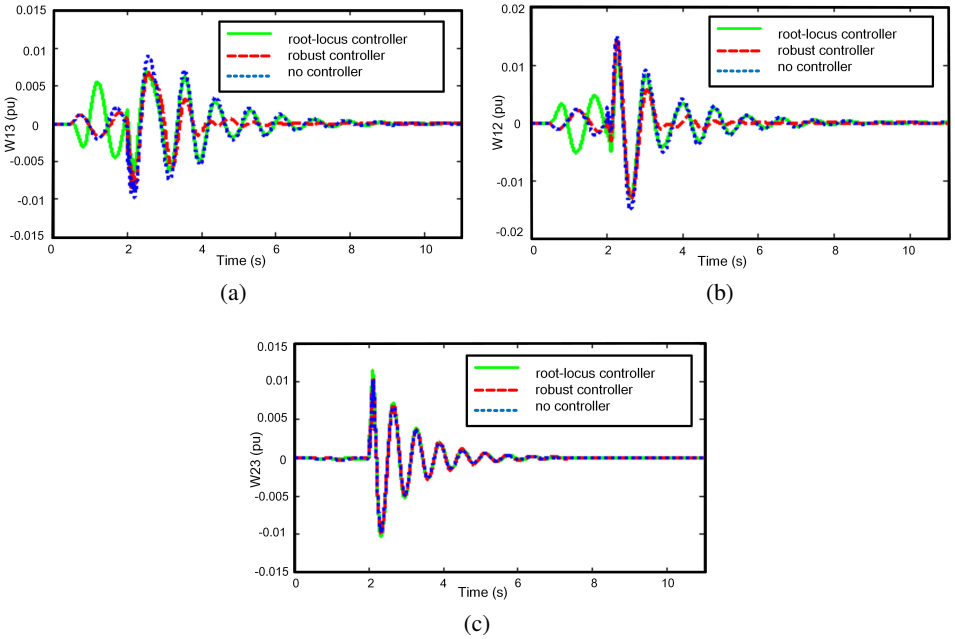

Fig. 9. Comparison of the control effect before and after the controller installation in case 2: comparison of the control effect based on $\omega 13$ (a); comparison of the control effect based on $\omega 12$ (b); comparison of the control effect based on $\omega 23$ (c)

It can be seen from Fig. 9 that in case 2, the root locus controller has little effect on suppressing system oscillation, while the robust controller can better suppress system oscillation. The reason is that the three-phase short-circuit fault causes a change in the system model, and the design of the additional damping controller was based on the transfer function of the system model. The robust performance is not considered in the design of the root locus controller, but the robust performance of the robust controller is relatively strong and insensitive to the change of the system model, exhibits strong adaptability, and can rapidly damp the LFO of the system.

The above research results indicate that if the receiving-end AC system undergoes LFO in the HMIDC system, the damping effect of adding an additional damping controller in VSC-HVDC is better than adding an additional damping controller in LCC-HVDC when the amount of power modulation is identical. When designing the additional damping controller, the robust controller designed using mixed H_2/H_∞ control theory has a better damping effect on LFO than the effect offered by the root locus controller based on classic root locus theory. The robust controller exhibits not only good robust performance but also strong adaptability to changes in the system operation model.

6. Conclusion

By fully utilizing the fast power regulation characteristics of an HVDC system, designing an additional damping controller is a workable measure to suppress the LFO of an AC system. TLS-ESPRIT can address the contradiction that strict control theory methods based on mathematical models are difficult to apply to actual engineering. It directly identifies the LFO modes and the transfer function of the system, which is of practical value for designing various types of additional controllers. According to the identified transfer function, the additional damping robust controller is designed using the mixed H_2/H_∞ control theory. It can not only place all the poles in a designated region to avoid the single-pole assignment inaccuracy caused by system uncertainty but also provide the controller with optimal and robust performance. This paper uses the LMI method to solve the controller problem to prevent the blindness of the controller parameter setting and can quickly acquire the controller parameters, and the calculation results are accurate and reliable. Based on the defined control sensitivity factor, if LCC-HVDC and VSC-HVDC have the same power modulation amount in the HMIDC system, we can conclude that VSC-HVDC has a better LFO damping effect than LCC-HVDC. Moreover, this paper also designs an additional damping controller based on the root locus method. A simulation in the time domain shows that the robust controller is superior to the damping controller of the root locus in suppressing LFO and restoring the stable operation of the system.

Acknowledgements

The authors gratefully acknowledge the National Natural Science Foundation of China (No. 51607158) and Star Sky Crowd Creation Space Incubation Project (DQX20200097).

References

[1] Bahrman M.P., Johnson B.K., *The ABCs of HVDC transmission technologies*, IEEE Power and Energy Magazine, vol. 5, no. 2, pp. 32–44 (2007), DOI: 10.1109/MPAE.2007.329194.

[2] Guo C., Liu W., Zhao J., Zhao C., *Impact of control system on small-signal stability of hybrid multi-infeed HVDC system*, IET Generation Transmission and Distribution, vol. 12, no. 19, pp. 4233–4239 (2018), DOI: 10.1049/iet-gtd.2018.5087.

[3] Bian X.Y., Geng Y., Lo K.L., Fu Y., Zhou Q.B., *Coordination of PSSs and SVC Damping Controller to Improve Probabilistic Small-Signal Stability of Power System With Wind Farm Integration*, IEEE Transactions on Power Systems, vol. 31, no. 3, pp. 2371–2382 (2016), DOI: 10.1109/TPWRS.2015.2458980.

[4] Salgotra A., Pan S., *A frequency domain model-based design of PSS and TCSC controller for damping the small signal oscillations in the power system*, International Transactions on Electrical Energy Systems, vol. 29, no. 3, pp. 1–18 (2019), DOI: 10.1002/etep.2742.

[5] Azizi N., Moradi Cheshmeh Beigi H., Rouzbehi K., *Optimal placement of direct current power system stabiliser (DC-PSS) in multi-terminal HVDC grids*, IET Gener. Transm. Distrib, vol. 14, no. 12, pp. 2315–2322 (2020), DOI: 10.1049/iet-gtd.2019.1224.

[6] He P., Wu X., Li C., Zheng M., Li Z., *Improvement of damping characteristics and index evaluation of a wind-PV-thermal-bundled power transmission system by combining PSS and SSSC*, Archives of Electrical Engineering, vol. 69, no. 3, pp. 705–721 (2020), DOI: 10.24425/aee.2020.133927.

[7] Dayalal Joshi K., Chandrakar V., *Power oscillation damping using ultracapcitor and voltage source based FACTS controllers*, 2017 IEEE International Conference on Electrical, Instrumentation and Communication Engineering (ICEICE), Karur, India, pp. 1–6 (2017), DOI: 10.1109/ICEICE.2017.8191878.

[8] Darabian M., Jalilvand A., *Designing a wide area damping controller to coordinate FACTS devices in the presence of wind turbines with regard to time delay*, IET Generation Transmission and Distribution, vol. 12, no. 13, pp. 1523–1537 (2018), DOI: 10.1049/iet-rpg.2017.0602.

[9] Pandey R.K., Gupta D.K., *Integrated Multi-stage LQR Power Oscillation Damping FACTS Controller*, CSEE Journal of Power And Energy Systems, vol. 4, no. 1, pp. 83–92 (2018), DOI: 10.17775/CSEEJPES.2016.00510.

[10] Liao K., Xu Y., Hai K.L., Qiao Y., *An ANN based damping controller for VSC-HVDC System*, 2017 Asian Conference on Energy, Power and Transportation Electrification (ACEPT), Singapore, pp. 1–6 (2017), DOI: 10.1109/ACEPT.2017.8168584.

[11] Azad S.P., Taylor J.A., Iravani R., *Decentralized Supplementary Control of Multiple LCC-HVDC Links*, IEEE Transactions on Power Systems, vol. 31, no. 1, pp. 572–580 (2016), DOI: 10.1109/TPWRS.2015.2393372.

[12] Ding Y., Liu T., Gao F. *et al*., *Multi-Channel HVDC Supplementary Damping Controller Design Based on Multi-Stage Linear Quadratic Regulator Method*, Transactions of China Electrotechnical Society, vol. 32, no. 6, pp. 76–84 (2017), DOI: 10.19595/j.cnki.1000-6753.tces.2017.06.010.

[13] Li B., Zhang Y., Li X. *et al*., *Design of Multi-Channel Additional Robust Controller for HVDC Transmission System*, Power System Technology, vol. 38, no. 4, pp. 858–864 (2014), DOI: 10.13335/j.1000-3673.pst.2014.04.006.

[14] Azad S.P., Iravani R., *Damping Interarea Oscillations Based on a Model Predictive Control (MPC) HVDC Supplementary Controller*, IEEE Transactions on Power Systems, vol. 28, no. 3, pp. 3174–3183 (2013), DOI: 10.1109/TPWRS.2013.2247640.

[15] Huang L., Xin H., Wang Z., *Damping Low-Frequency Oscillations Through VSC-HVDC Stations Operated as Virtual Synchronous Machines*, IEEE Transactions on Power Electronics, vol. 34, no. 6, pp. 5803–5818 (2018), DOI: 10.1109/TPEL.2018.2866523.

[16] Farhang P., Tirtashi M.R., Noroozian R. *et al*., *Combined design of VSC-HVDC and PSS controllers for LFO damping enhancement*, Transactions of the Institute of Measurement and Control, vol. 36, no. 4, pp. 529–540 (2014), DOI: 10.1177/0142331213509832.

[17] Hu B., Wang X., Teng Y., Ai P., *Wide-area damping control system design with multi-HVDC based on state space model identification and geometric index*, 2017 36th Chinese Control Conference (CCC), Dalian, pp. 10540–10546 (2017), DOI: 10.23919/ChiCC.2017.8029036.

[18] Roberson D., O'Brien J., *Loop shaping of a wide-area damping controller using HVDC*, 2017 IEEE Power and Energy Society General Meeting, Chicago, IL, p. 2354–2361 (2017), DOI: 10.1109/TPWRS.2016.2608356.

[19] Agnihotri P., Kulkarni A., Gole A., Archer B., Weekes T., *A Robust Wide-Area Measurement-Based Damping Controller for Networks with Embedded Multiterminal and Multi-infeed HVDC Links*, in IEEE Transactions on Power Systems, vol. 32, no. 5, pp. 3884–3892 (2017), DOI: 10.1109/PESGM40551.2019.8973954.

[20] Wang X., Wang Y., Li X. *et al.*, *Controllability Sensitive Points of Matrix Pencil Identification Multi-HVDC Systems*, Proceedings of the CSU-EPSA, vol. 25, no. 1, pp. 29–33 (2013).

[21] Guo L., Liu T., Cheng D. *et al.*, *Study on digging the most sensitive control point of multi-terminal HVDC system*, Power System Protection and Control, vol. 41, no. 10, pp. 7–12 (2013), DOI: 10.7667/j.issn.1674-3415.2013.10.002.

[22] Lin Q., Li X., Wang X. *et al.*, *Sensitive point digging for additional damping control in multi-HVDC system*, Electric Power Automation Equipment, vol. 34, no. 7, pp. 76–80, (2014), DOI: 10.7667/j.issn.1674-3415.2013.10.002.

[23] Chen J., Jin T., Mohamed A.M., Wang M., *An Adaptive TLS-ESPRIT Algorithm Based on an S-G Filter for Analysis of Low Frequency Oscillation in Wide Area Measurement Systems*, IEEE Access, vol. 7, pp. 47644–47654 (2019), DOI: 10.1109/ACCESS.2019.2908629.

[24] Wang L., Li F., Yin C. *et al.*, *Analysis of asymmetric fault commutation failure in an HVDC system with DC current variation*, Power Syst. Prot. Control, vol. 49, no. 1, pp. 17–23 (2021), DOI: 10.19783/j.cnki.pspc.200054.